Characterizing Hostrocks and Alteration Footprints at the Lorraine Alkalic Copper-Gold Porphyry Deposit, North-Central British Columbia (Part of NTS 093N/14)

H. Xu[1], Department of Earth, Ocean and Atmospheric Sciences, The University of British Columbia, Vancouver, British Columbia, dxu@eoas.ubc.ca

S. Barker, Department of Earth, Ocean and Atmospheric Sciences, The University of British Columbia, Vancouver, British Columbia

F. Bouzari, Department of Earth, Ocean and Atmospheric Sciences, The University of British Columbia, Vancouver, British Columbia

C. Harraden, Department of Earth, Ocean and Atmospheric Sciences, The University of British Columbia, Vancouver, British Columbia

M. Manor, NorthWest Copper Corp. and Department of Earth, Ocean and Atmospheric Sciences, The University of British Columbia, Vancouver, British Columbia

Xu, H., Barker, S., Bouzari, F., Harraden, C. and Manor, M. (2024): Characterizing hostrocks and alteration footprints at the Lorraine alkalic copper-gold porphyry deposit, north-central British Columbia (part of NTS 093N/14); *in* Geoscience BC Summary of Activities 2023, Geoscience BC, Report 2024-01, p. 11–22.

Introduction

Copper is currently one of the most widely used metals, essential to the construction of infrastructure and the production of electronics, vehicles and renewable energy systems (Schlesinger et al., 2011; Mudd et al., 2013). In the 20th century, copper demand increased dramatically and copper resources will become even more critical for future society, due to the global promotion of the green energy transition (Schipper et al., 2018). The increase in demand will require the discovery of new copper resources. Porphyry copper-gold deposits are considered one of the primary repositories of global copper resources (Mudd et al., 2013; Mudd and Jowitt., 2018). Porphyry deposits are generally associated with a series of oxidized calcalkalic or alkalic subvolcanic intrusions at convergent margins that exhibit distinctive hydrothermal alteration zonation patterns (Cooke et al., 2007; Sillitoe, 2010). Although alkalic deposits typically have a smaller footprint than calcalkalic deposits, alkalic porphyry deposits play an important role in copper exploration due to their high metal grades (Bissig and Cooke, 2014; Müller and Groves, 2019; Kwan and Müller, 2020). The alkalic porphyry province in British Columbia (BC), includes several world-famous deposits (Figure 1) such as Galore Creek, Mount Milligan, Mount Polley and Lorraine (Lang et al., 1995; Cooke et al., 2007; Bouzari et al., 2016).

The Lorraine porphyry Cu-Au deposit is located about 300 km northwest of Prince George and is among several deposits that highlight the significant base- and precious-metal endowment of the Canadian Cordillera. The resource comprises the Lower Main zone, the Upper Main zone and the Bishop zone. Previous studies have focused mainly on the Lower Main zone (Bath et al., 2014; Devine et al., 2014) but less work has been conducted on the other two zones. These zones are hosted by a wide range of felsic to ultramafic rocks, which are variably altered and mineralized. The aim of this study is to characterize different rock types and alteration assemblages across the three zones to fill the knowledge gaps from previous work and contribute to exploration of the Lorraine deposit.

Geological Setting

The Lorraine alkalic porphyry Cu-Au deposit is located in the Triassic–Jurassic Quesnel arc of north-central BC (Figure 2). The area around the Lorraine deposit is composed of volcanic and sedimentary rocks of the Late Triassic Takla Group and intruded by Late Triassic to mid-Cretaceous plutons of the Hogem batholith (Nixon and Peatfield, 2003; Bath et al., 2014; Devine et al., 2014; Ootes et al., 2020).

The Hogem batholith around the Lorraine area is subdivided into five suites comprising, from oldest to youngest: 1) Late Triassic to Early Jurassic Hogem granodiorite in the central area; 2) Late Triassic to Early Jurassic diorite, monzodiorite and quartz monzodiorite of the Thane and Detni plutons; 3) the Early Jurassic Duckling Creek syenite complex, which hosts the Lorraine deposit; 4) Early to mid-Cretaceous granodiorite and granite of the Osilinka intrusions in the northern section of the Hogem batholith; and

[1] *The lead author is a 2023 Geoscience BC Scholarship recipient.*

This publication is also available, free of charge, as colour digital files in Adobe Acrobat® PDF format from the Geoscience BC website: https://geosciencebc.com/updates/summary-of-activities/.

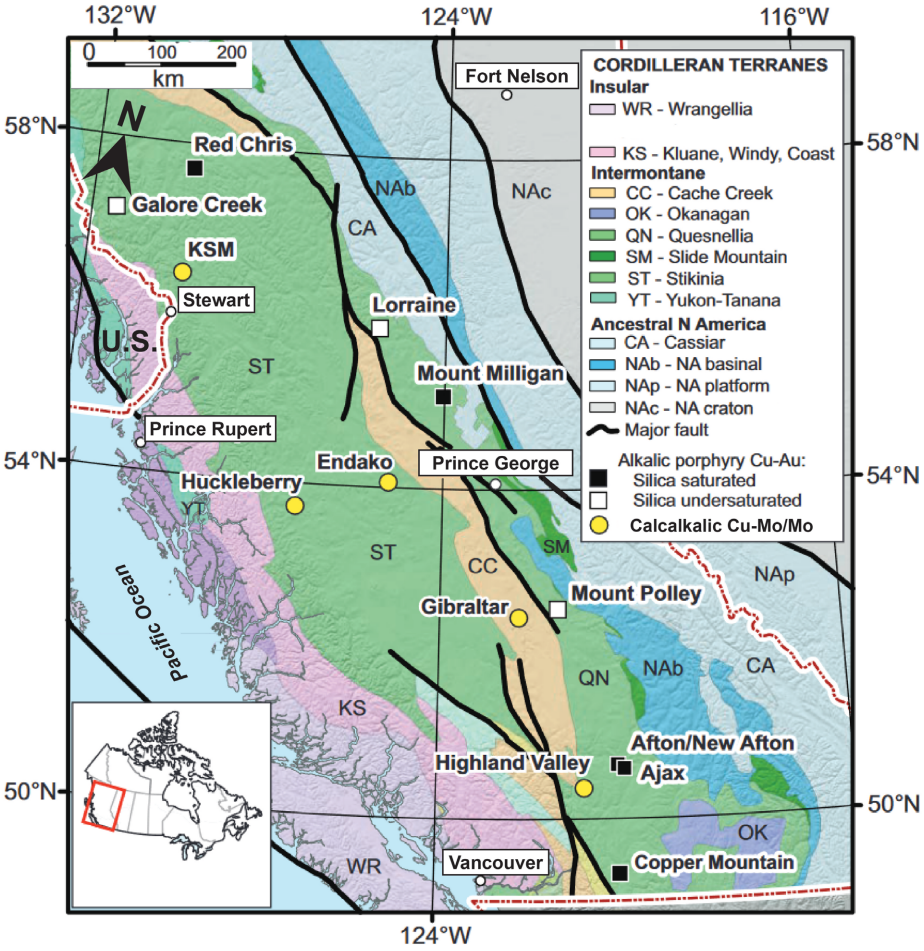

Figure 1. Tectonostratigraphic terranes and location of major porphyry deposits in British Columbia (modified from Bouzari et al., 2016).

5) Early to mid-Cretaceous granodiorite, quartz diorite and monzodiorite of the Mesilinka pluton in the northwestern part of the Hogem batholith (Figure 2; Nixon and Peatfield, 2003; Bath, 2010; Bath et al., 2014).

The Duckling Creek syenite complex is a multiphase alkalic intrusive complex that trends generally northwest and is approximately 30 km long by 5 km wide. Its southeastern boundary is the north-northwest-trending Duckling fault, to the east of which lie the Rhonda-Dorothy gabbro-diorite and Takla Group volcanic rocks. The Duckling Creek syenite complex is composed of syenite, pyroxenite, monzonite and diorite. Previous studies (Bath, 2010; Bath et al., 2014; Devine et al., 2014) have classified these rock types into three phases based on the relative timing of emplacement with respect to mineralization. Phase 1 rocks are regarded as the hostrock for mineralization and are composed of silica-undersaturated syenite and pyroxenite. Devine et al. (2014) proposed that phase 1 rocks dip southwest due to tilting following the main stage of mineralization. Phase 2 rocks exhibit similar mineralogy to phase 1 rocks and are composed of unmineralized silica-undersaturated syenite and pyroxenite. Late unmineralized phase 3 silica-saturated leucosyenite and pegmatitic dikes are compositionally distinct from phase 1 and 2 units. According to previous studies (Bath, 2010; Bath et al., 2014; Devine et al., 2014), the sulphide zones (Figure 3) are defined by bornite-chalcocite cores, ringed by chalcopyrite-dominant zones, with outer pyrite-dominant zones. The alteration assemblages were interpreted by Devine et al. (2014) as pervasive K-feldspar–biotite alteration (potassic alteration) in the core surrounded by albite-diopside-magnetite alteration (calcpotassic alteration). Distinctive patterns of sulphide and alteration zonation at the Lorraine deposit have been documented in previous work, in which it is further classified as a tilted alkalic porphyry-style deposit.

Methodology

Thin-section analysis to characterize rock types and alteration assemblages to better understand the characteristics of the Lorraine deposit is the focus of this study. Thin sections were provided by the sponsor company, NorthWest Copper Corp., and were cut from company-selected

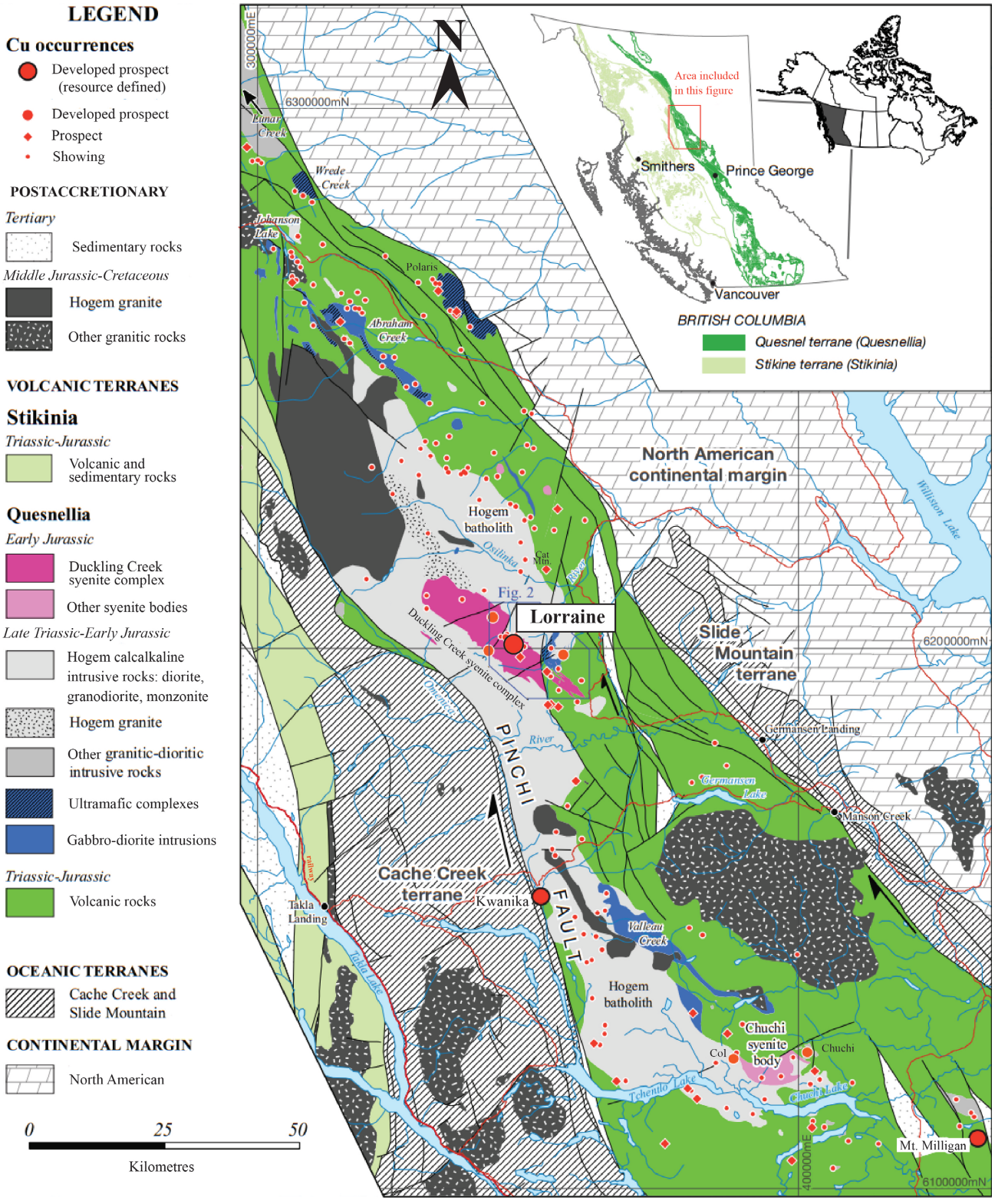

Figure 2. Geology of the central Quesnel terrane, highlighting the Hogem batholith, the Duckling Creek syenite complex and the Lorraine deposit (modified from Devine et al., 2014). The term 'Tertiary' used in this figure is a historical term. The International Commission on Stratigraphy recommends using 'Paleogene' (comprising the Paleocene to Oligocene epochs) and 'Neogene' (comprising the Miocene and Pliocene epochs). The author used the term 'Tertiary' because it was used in the source material for this figure. All co-ordinates are in UTM Zone 10, NAD 83.

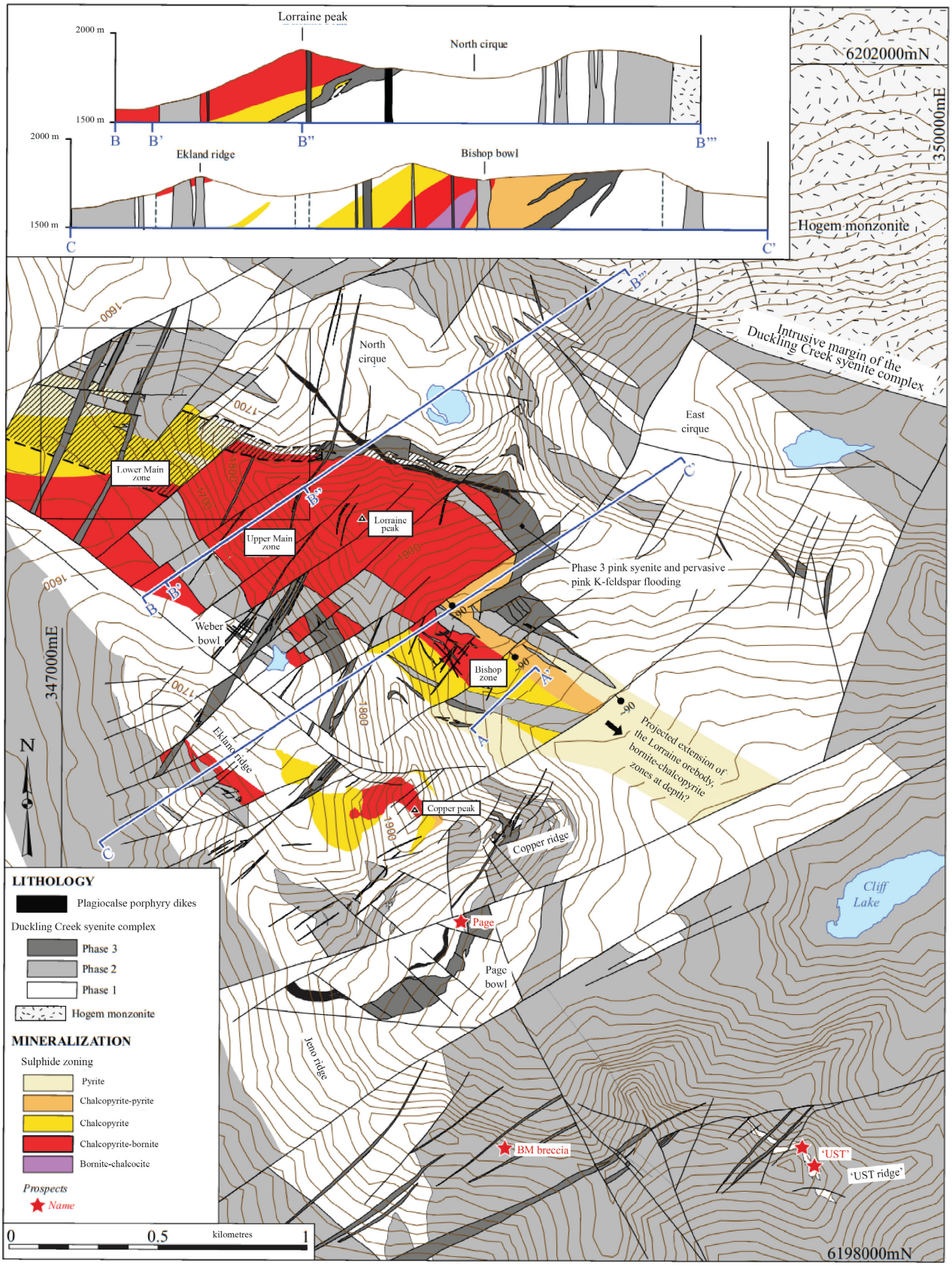

Figure 3. Geology and cross-sections of the Lorraine deposit, highlighting the distribution of different phases of intrusion and sulphide-alteration zonation (modified from Devine et al., 2014). Place names with the generic in lower case are unofficial. All co-ordinates are in UTM Zone 10, NAD 83.

Table 1. Selected drillholes and number of thin sections selected from each drillhole in the Lower Main zone, Upper Main zone and Bishop zone of the Lorraine deposit.

Lower Main zone		Upper Main zone		Bishop zone	
Hole ID	Thin sections	Hole ID	Thin sections	Hole ID	Thin sections
LOR-01-56	2	LOR-01-50	5	LOR-91-07	2
LOR-01-60	3	LOR-01-51	3	LOR-91-11	1
LOR-02-66	1	LOR-22-132	1	LOR-94-06	1
		LOR-22-133	1	LOR-96-43	6
		LOR-22-136	2	LOR-96-44	2
Total	6	Total	12	Total	12

Table 2. Classification of pyroxenite and syenite, with corresponding mineral modal abundance determined from the analysis of thin sections from drillcore samples from the Lorraine deposit.

Pyroxenite				
	diopside	biotite	K-feldspar	Accessory minerals (Ap, Mag, Ttn)
Biotite clinopyroxenite	60–85%	5–40%	0–20%	<20%
Feldspathic biotite	40–60%	10–35%	20–40%	<20%

Syenite				
	diopside + biotite	plagioclase	K-feldspar	Accessory minerals (Ap, Mag, Ttn)
Melanocratic syenite	40–60%	0–5%	40–60%	<20%
Mesocratic syenite	15–40%	0–10%	60–75%	<15%
Leucocratic syenite	0–15%	0–10%	85–95%	<5%

drillcore samples collected from three drillholes in the Lower Main zone, five holes in the Upper Main zone and five holes in the Bishop zone (Table 1). Thirty thin sections with various grades of mineralization were selected from these thirteen drillholes (Figure 4), including six thin sections from the Lower Main zone, twelve thin sections from the Upper Main zone and twelve thin sections from the Bishop zone. These samples include examples of different rock types from different zones at the Lorraine deposit, which will help develop further understanding of the lithological relationships across the three zones.

The selected samples were digitally scanned at the Mineral Deposit Research Unit of The University of British Columbia (UBC) using the Zeiss Axioscan 7 Geo automated petrography system at 5x magnification. Digital images exhibit the complete optical view of thin sections for precise mineral abundance estimation and help to illustrate mineral texture at a coarser scale. The digital thin-section images were analyzed using the ZEN lite software (3.8 version) from Zeiss. Selected thin sections were sent to the UBC microbeam and X-ray laboratory to map major elements using scanning electron microscopy (SEM). All SEM images were obtained using an energy level of 20 kV, at a working distance of 10 mm, a map resolution of 750 by 750 pixels and a pixel size of 3 μm.

Rock-Type Characterization

According to the ultramafic rock classification scheme from Le Maitre (2002), pyroxenite samples from Lorraine are classified as clinopyroxenite due to the presence of diopside and the absence of olivine and orthopyroxene (Bath, 2010). Based on the abundance of feldspars in digital thin-section images the clinopyroxenite can be subdivided into biotite clinopyroxenite and feldspathic biotite clinopyroxenite (Table 2).

Biotite clinopyroxenite (Figure 5a, b) contains 60–85% green, cumulus, euhedral to subhedral diopside; 5–40% yellow to dark brown, pleochroic, intercumulus, subhedral to anhedral biotite; 0–20% fine-grained intercumulus, anhedral K-feldspar; and <5% subhedral to anhedral plagioclase. Accessory minerals are euhedral apatite (3–15%), magnetite (5–10%) and subhedral to anhedral titanite (0–7%). Disseminated bornite-chalcopyrite is locally present in biotite clinopyroxenite. Two thin sections are classified as biotite clinopyroxenite, one from the Upper Main zone and the other from the Bishop zone.

Feldspathic biotite clinopyroxenite (Figure 5c, d) is differentiated from biotite clinopyroxenite by the abundance of K-feldspar. It is characterized by 40–60% euhedral to subhedral diopside, 20–40% medium-grained anhedral K-feldspar, 10–35% subhedral to anhedral intercumulus biotite and 2–7% subhedral to anhedral plagioclase. Accessory

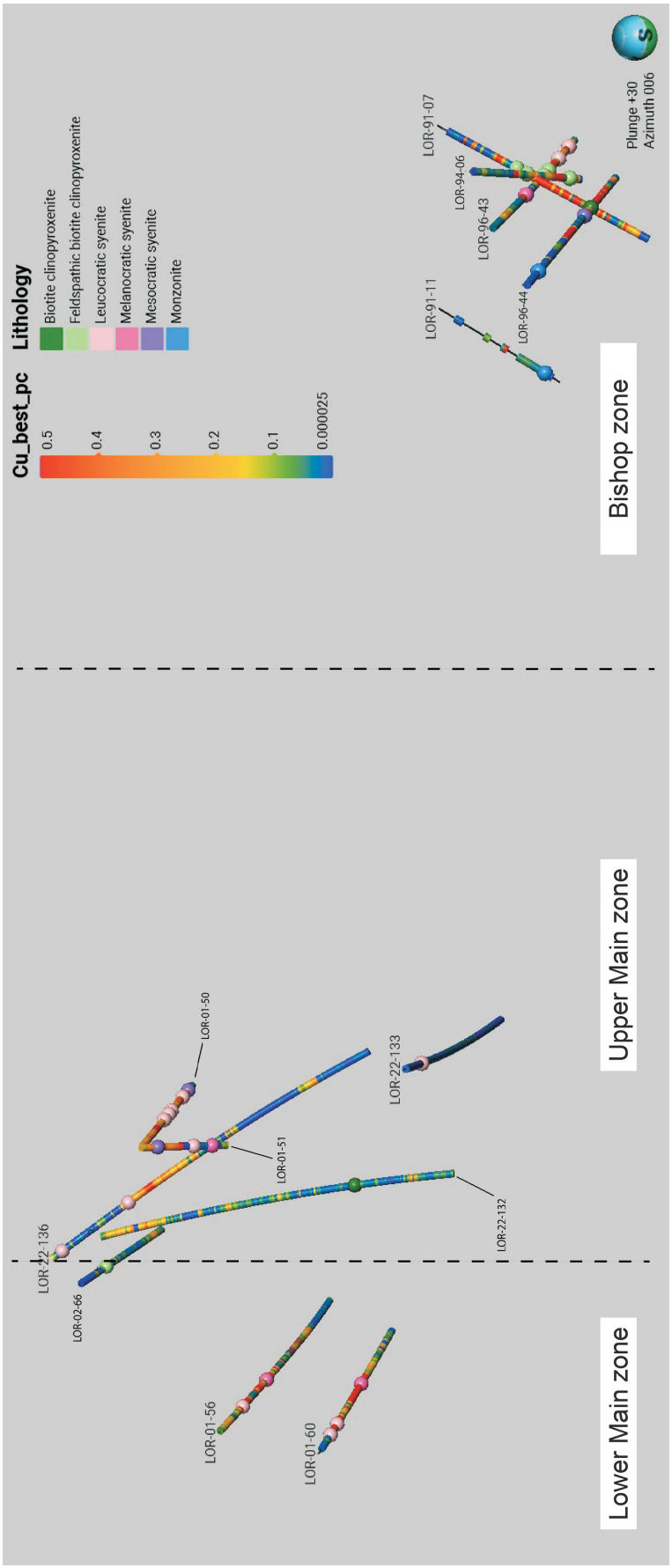

Figure 4. Geospatial distribution of selected drillholes at the Lorraine deposit; with the different rock types represented by the coloured nodes and the amount of mineral present (Cu_best_pc) represented by the coloured drillhole segments between the nodes (copper content ranging between 0.000025 and 0.5 %).

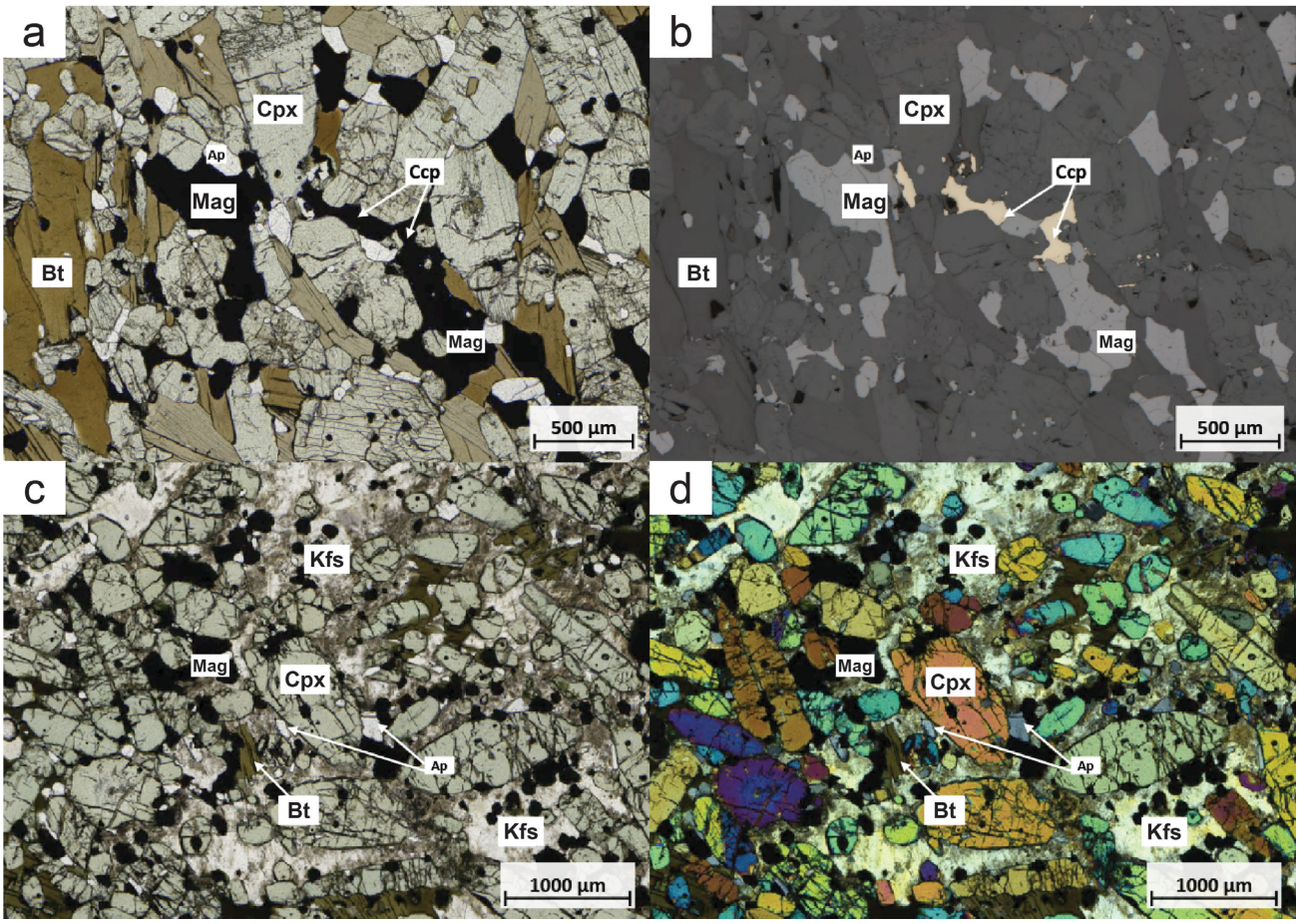

Figure 5. Photomicrographs of clinopyroxenite in thin sections from drillcore samples from the Lorraine deposit: **a)** image in plain-polarized light of biotite and diopside showing cumulus texture from biotite clinopyroxenite (sample 4653387, drillhole LOR-22-132 at 279.8 m, Upper Main zone); **b)** same image as (a) in reflected light; **c)** image in plane-polarized light of cumulus diopside with intercumulus K-feldspar and biotite from feldspathic biotite clinopyroxenite (sample 4653564, drillhole LOR-02-66 at 49.8 m, Lower Main zone); **d)** same image as (c) in cross-polarized light. Abbreviations: Ap, apatite; Bt, biotite; Ccp, chalcopyrite; Cpx, clinopyroxene; Kfs, K-feldspar; Mag, magnetite.

minerals comprise euhedral apatite (3–10%), magnetite (3–8%) and subhedral to anhedral titanite (<3%). Potassium-feldspar commonly has turbid boundaries. The cumulate texture of both types of clinopyroxenite is consistent across all three zones at the Lorraine deposit.

In mineralized clinopyroxenite, copper sulphides precipitate interstitially to form primary diopside and biotite and replace K-feldspar. The diopside and biotite grains that are in contact with sulphides are commonly unaltered and have sharp grain boundaries. Six thin sections are classified as feldspathic biotite clinopyroxenite. Five of these came from the Bishop zone and a single one from the Lower Main zone.

According to the felsic rock classification scheme of Le Maitre (2002), syenite at Lorraine is divided into three groups (Table 2) based on the abundance of mafic minerals (diopside and biotite): leucocratic syenite, mesocratic syenite and melanocratic syenite. Leucocratic syenite (Figure 6a, b) is characterized by 85–95% cumulus anhedral K-feldspar, 0–10% euhedral to subhedral diopside, 0–8% anhedral biotite and <10% subhedral to anhedral plagioclase, with accessory magnetite (<5%). Mesocratic syenite (Figure 6c) is characterized by 60–75% anhedral K-feldspar, 15–30% euhedral to subhedral diopside, 8–15% anhedral biotite and 3–8% subhedral to anhedral plagioclase, with minor magnetite (5–7%) and apatite (3–5%). Melanocratic syenite (Figure 6d) is characterized by 40–60% K-feldspar, 35–55% euhedral to subhedral diopside, 10–25% anhedral biotite and <5% plagioclase, with accessory magnetite (<10%) and euhedral apatite (5–8%). Trace titanite, rutile and zircon are present in some of the syenite samples. Sulphides are observed in all three types of syenite, mostly as disseminated chalcopyrite-pyrite. Bornite-chalcopyrite is also observed in some of the thin sections. Disseminated chalcopyrite (2–3 vol %) is commonly found in leucocratic syenite but is less common (<1 vol %) in mesocratic and melanocratic syenite. The sample suite includes thirteen leucocratic syenite samples, three mesocratic syenite samples and four melanocratic

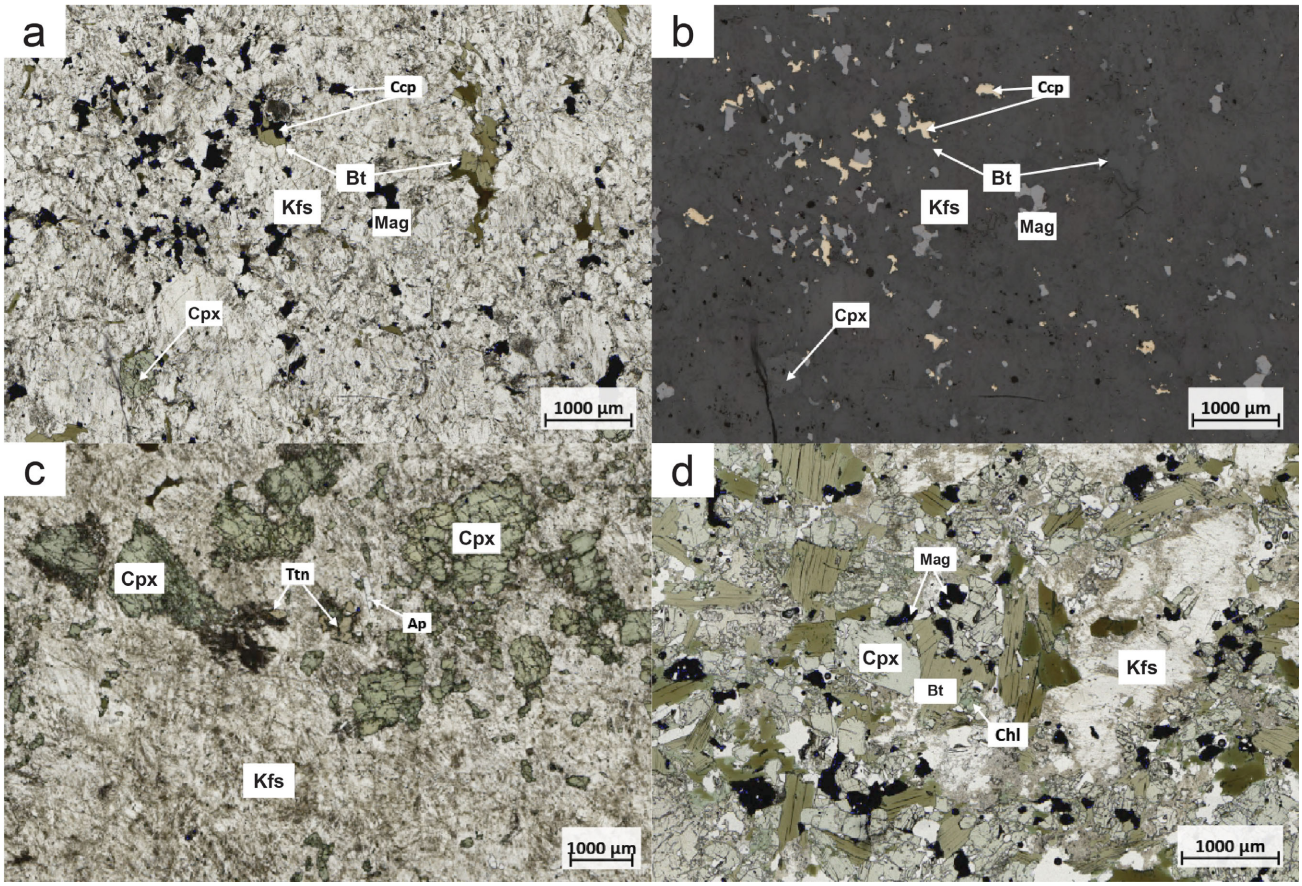

Figure 6. Photomicrographs of syenite in thin sections from drillcore samples from the Lorraine deposit: **a)** image in plane-polarized light of leucocratic syenite with <10% of mafic minerals (sample 4653394, drillhole LOR-96-43 at 167.6 m, Bishop zone); **b)** same image as (a) in reflected light; **c)** image in plane-polarized light of mesocratic syenite with 10–50% of mafic minerals (drillhole LOR-01-50 at 154.7 m, Upper Main zone); **d)** image in plane-polarized light of melanocratic syenite with >50% of mafic minerals (sample 4653596, drillhole LOR-01-51 at 84.3 m, Upper Main zone). Abbreviations: Ap, apatite; Bt, biotite; Ccp, chalcopyrite; Chl, chlorite; Cpx, clinopyroxene; Kfs, K-feldspar; Ttn, titanite.

syenite samples. Leucocratic syenite samples are mostly from the Lower Main zone and Upper Main zone except for two samples from the Bishop zone. Mesocratic syenites are mostly from the Upper Main zone, except for one sample from the Bishop zone. Two melanocratic syenite samples came from the Lower Main zone, whereas the other two samples came from the Upper Main zone and the Bishop zone, respectively (Figure 4).

Alteration Minerals

Four alteration minerals were studied: biotite, epidote, garnet and albite. In the selected thin-section suite, biotite is divided into three types. The first, Bt 1, is commonly present in pyroxenite, and in mesocratic and melanocratic syenites (Figure 7a). This type of biotite is commonly medium grained, subhedral to anhedral to locally poikilitic, with diopside and apatite chadacrysts, yellow to dark brown pleochroic and sometimes exhibits perfect cleavages, whereas Bt 2 is very fine grained and lacks visible cleavages. Diopside along fractures is most commonly replaced by Bt 2 as thin biotite veinlets and along diopside grain boundaries as biotite patches before being subsequently partially to completely replaced by chlorite (Figure 7a). Results from semi-quantitative SEM analysis indicate that coarse-grained biotite has higher Fe (27–29%) and Ti (2.9–5.2%) contents but a lower Mg content (11.9–13.4%) than the very fine-grained biotite, which has lower Fe (about 23%) and Ti (0.5–0.7%) contents but a higher Mg (15.9–18%) content. Finally, Bt 3 is present in some leucocratic syenite samples (Figure 7b). This third type of biotite is fine grained, yellow to reddish-brown pleochroic and has imperfect cleavages in some cases; it is commonly associated with euhedral chalcopyrite-pyrite.

Garnet and epidote are commonly present in mineralized feldspathic biotite clinopyroxenite and mineralized syenite at the Lorraine deposit. The garnet is fine grained, light brown (Figure 8a), euhedral to subhedral, of high relief, zoned, optically anisotropic, with first-order grey to yellow interference colours (Figure 8b), and is typically associated with epidote. Garnet appears to replace both intercumulus

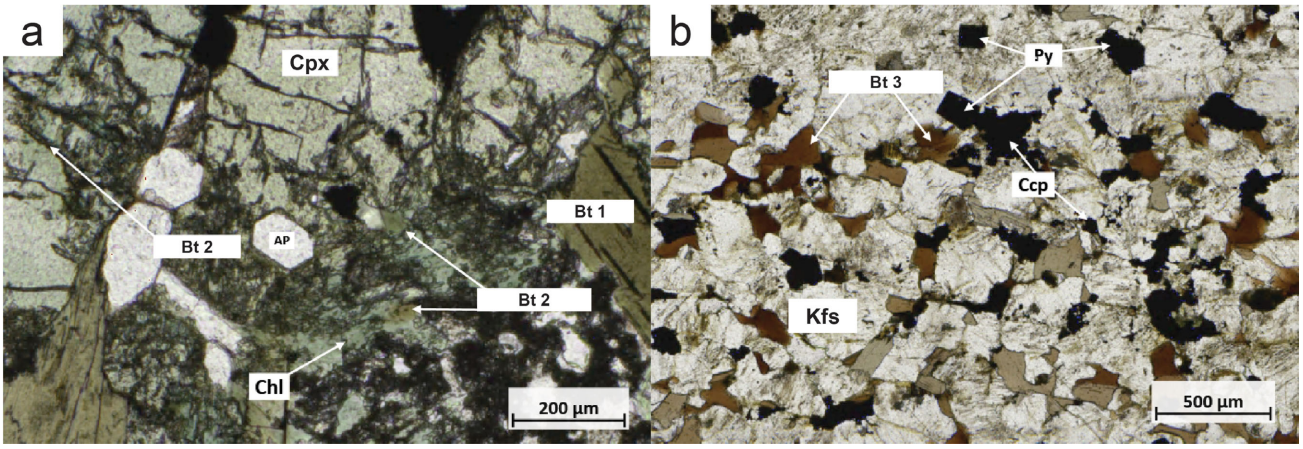

Figure 7. Photomicrographs of biotite alteration in thin sections from drillcore samples from the Lorraine deposit: **a)** image in plane-polarized light of melanocratic syenite with two types of biotite, the first (Bt 1) being medium grained, euhedral to subhedral and exhibiting perfect cleavages, whereas the second (Bt 2) grows along diopside grain fractures and along diopside grain boundaries to form biotite veinlets and biotite patches before being subsequently altered to chlorite (drillhole LOR-96-43 at 83.8 m, Bishop zone); **b)** image in cross-polarized light of leucocratic syenite with reddish-brown biotite (Bt 3) closely associated with chalcopyrite and pyrite (sample 3678951, drillhole LOR-22-136 at 102.6 m, Upper Main zone). Abbreviations: Ap, apatite; Bt, biotite; Ccp, chalcopyrite; Chl, chlorite; Cpx, clinopyroxene; Kfs, K-feldspar; Py, pyrite.

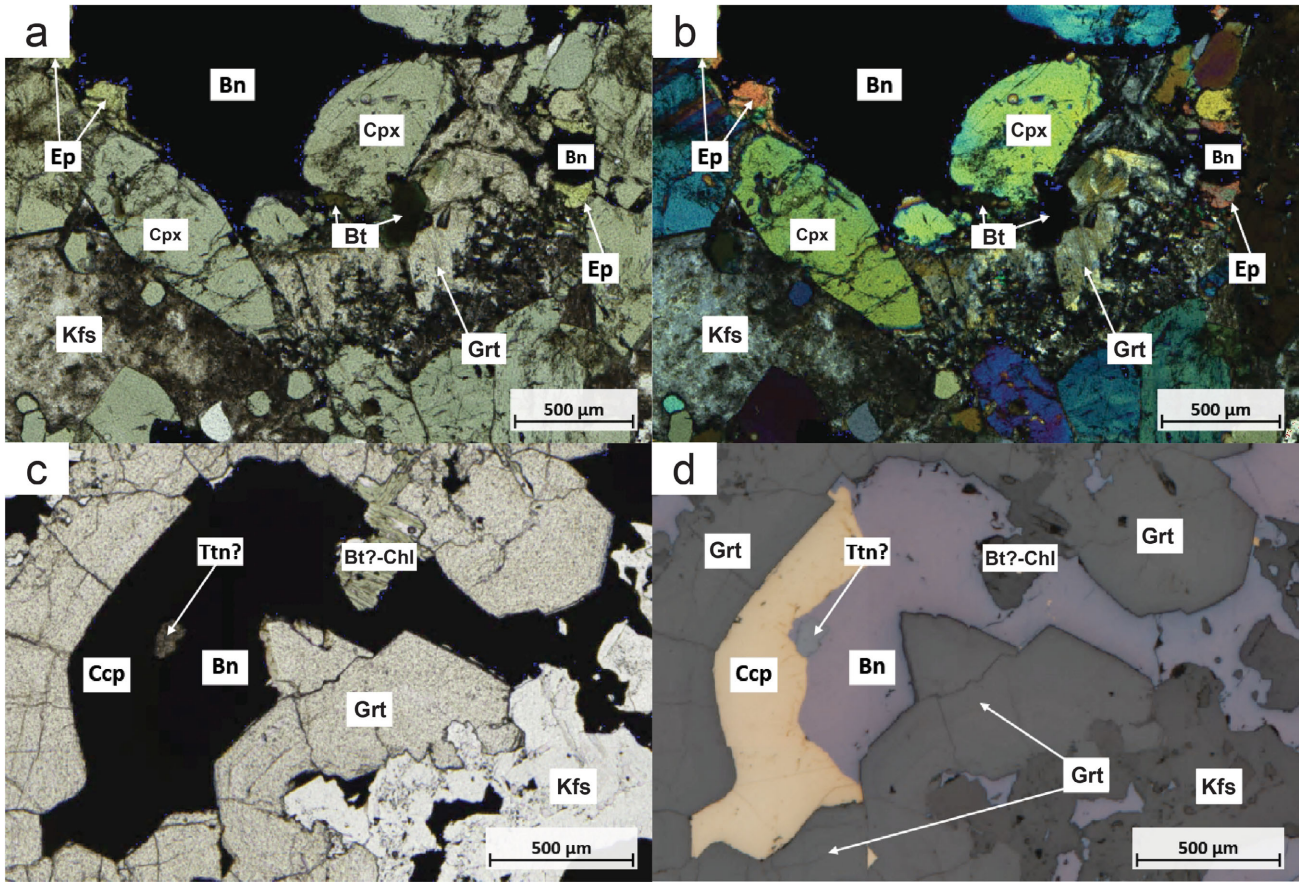

Figure 8. Photomicrographs of epidote-garnet alteration in thin sections from drillcore samples from the Lorraine deposit: **a)** image in plane-polarized light of feldspathic biotite clinopyroxenite with epidote-garnet assemblage, characterized by light brown, high-relief garnets that replace intercumulus K-feldspar and epidote in contact with bornite as well as weakly altered surrounding diopside (sample 4653542, drillhole LOR-91-07 at 89.3 m, Bishop zone); **b)** same image as (a) in cross-polarized light; **c)** image in plane-polarized light of bornite-chalcopyrite filling open space and sharp contacts with surrounding hydrothermal garnet, which indicates that epidote-garnet alteration is pre- or synmineralization (drillhole LOR-91-11 at 120.2 m, Bishop zone); **d)** same image as (c) in reflected light. Abbreviations: Ap, apatite; Bt, biotite; Bn, bornite; Ccp, chalcopyrite; Chl, chlorite; Cpx, clinopyroxene; Ep, epidote; Grt, garnet; Kfs, K-feldspar; Ttn, titanite.

K-feldspar in pyroxenite and K-feldspar in syenite to form irregular contacts with surrounding K-feldspar (Figure 8a, b). Garnet-associated copper sulphides tend to have sharp contacts with the surrounding garnet, exhibiting void-filling textures (Figure 8c, d). Epidote is euhedral, fine grained, of moderate relief and is yellow pleochroic to transparent (Figure 8a, b). Epidote overprints both K-feldspar and diopside in pyroxenite and syenite. Garnet is commonly associated with epidote in mineralized samples, but epidote also occurs where sulphide mineralization is not present.

Alteration albite is difficult to identify petrographically because it is optically similar to primary K-feldspar (Figure 9a); in pyroxenite, the presence of albite was only detected by SEM analysis. Albite commonly replaces intercumulus K-feldspar to form albite patches (Figure 9a, b). In mineralized pyroxenite, albite locally replaces

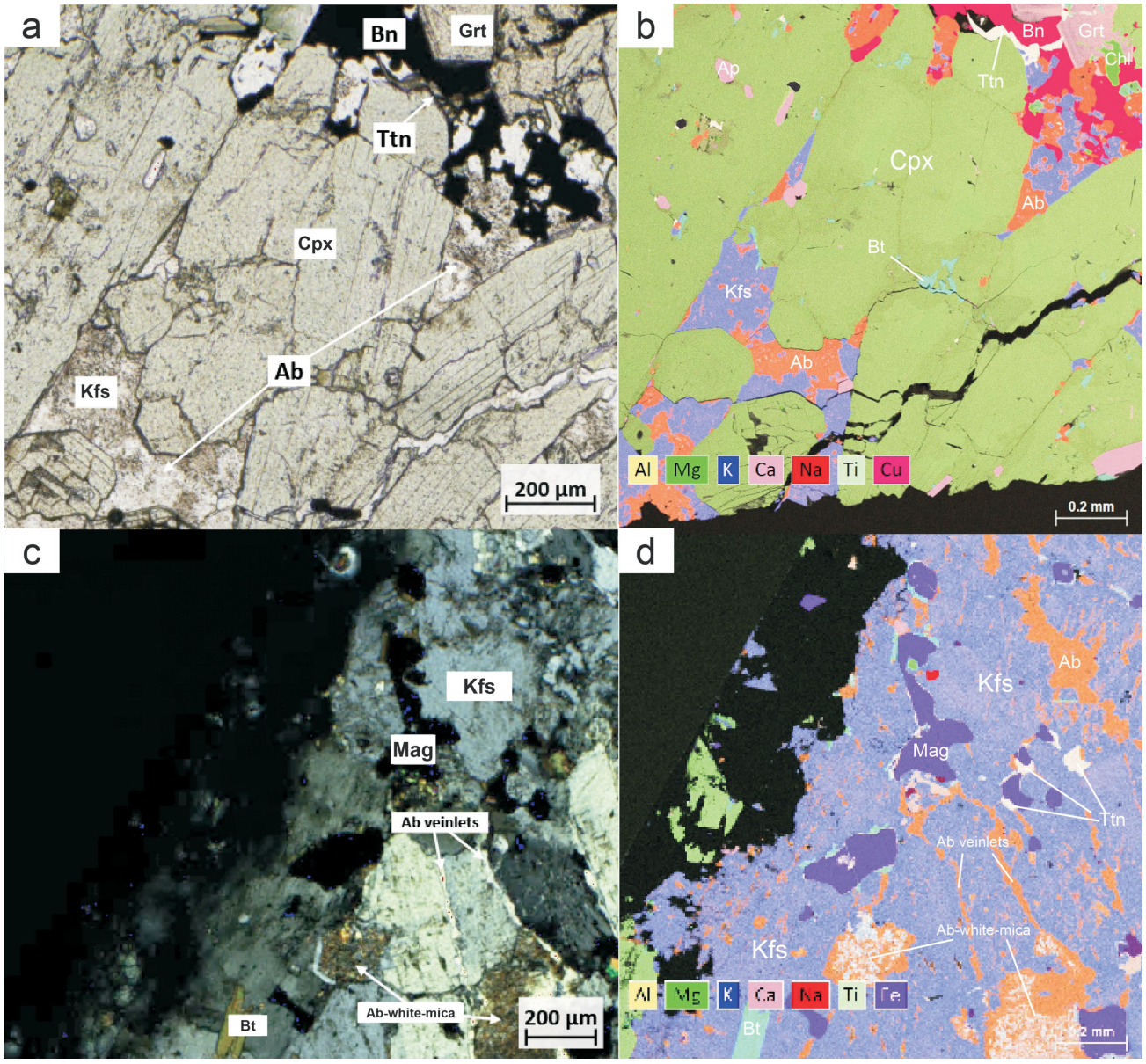

Figure 9. Photomicrographs and scanning electron microscope (SEM) images of albite alteration in thin sections from drillcore samples from the Lorraine deposit: **a)** image in plane-polarized light of feldspathic biotite clinopyroxenite with both garnet alteration and albite alteration, which is difficult to identify due to its similarity to primary K-feldspar (sample 4653542, drillhole L91-07 at 89.3 m, Bishop zone); **b)** same image as (a) but showing, as detected by SEM, that albite altered intercumulus K-feldspar and overprinted garnet have blurry contacts with bornite; **c)** image in cross-polarized light of leucocratic syenite with albite alteration (optically identified due to the relatively higher relief and interference colour) that commonly occurs along K-feldspar grain boundaries and at times within K-feldspar grains, whereas plagioclase is shown to be strongly to completely altered to albite-white mica (sample 4653394, drillhole LOR-96-43 at 167.6 m, Bishop zone,); **d)** SEM image of (c). Abbreviations: Ab, albite; Ap, apatite; Bt, biotite; Bn, bornite; Chl, chlorite; Cpx, clinopyroxene; Grt, garnet; Kfs, K-feldspar; Ttn, titanite.

garnet alteration (Figure 9b, upper right corner). In syenite, albite has relatively higher relief and first-order birefringence compared to surrounding K-feldspar. It commonly occurs along K-feldspar grain boundaries as albite veinlets and can be identified from both photomicrographs and SEM images (Figure 9c, d). The albite veinlets are thin (about 20–50 μm wide), and the contacts with K-feldspar are usually indistinct. The K-feldspar is also weakly altered to form fine albite patches within grains, whereas plagioclase (identified by remnants of polysynthetic twinning) is strongly to completely altered by albite and white mica.

Discussion

The aim of this study is to characterize the mineralogy of pyroxenite and syenite at the Lorraine deposit; texturally and geochemically evaluate the origins of minerals; and assess the relationship between different types of alteration and mineralization. In previous studies of the area (Bath et al., 2014; Devine et al., 2014), it was proposed that pervasive biotite alteration is the most common alteration style and that it is closely associated with mineralization. The petrography reported herein indicates that biotite from leucocratic syenite (Bt 3, Figure 7b) correlates strongly with mineralization, whereas biotite in pyroxenite, mesocratic syenite and melanocratic syenite (Bt 1 and Bt 2, Figure 7a) shows less spatial correlation with mineralization. Although the three types of biotite identified in this study are texturally and geochemically distinct from each other, the current results are too sparse to determine if they were formed by igneous or hydrothermal processes. There is insufficient evidence to support the assumption that Bt 1 and Bt 2 are associated with mineralization, whereas Bt 3 is strongly correlated with copper sulphide in leucocratic syenite.

Epidote-garnet alteration was documented in previous studies (Devine et al., 2014) as two separate alteration types. Devine et al. (2014) proposed that albite-epidote alteration was present in postmineralized intrusions and that garnet alteration locally occurred in distal postmineralization melanocratic syenite. Observations from the present study suggest that epidote-garnet alteration is more common than previously documented and closely correlates with mineralization. The uncommon anisotropic garnet detected by SEM analysis shows similar optical properties to hydrothermal garnet from the Oslo Rift of southern Norway documented in Jamtveit (1991) and Jamtveit et al. (1995), which implies a hydrothermal origin for the grossular-andradite garnet at the Lorraine deposit. The sharp contacts between copper sulphides and garnet (Figure 8c, d) indicate that garnet alteration is pre- or syn-mineralization. Although garnet and epidote are strongly associated with each other in mineralized samples, epidote is also associated with mineralization in areas where no garnet is present. This suggests that there are two separate phases of alteration at the Lorraine deposit: epidote-garnet alteration and epidote-only alteration. Bath (2010) proposed that albite alteration is present in distal zones and relatively uncommon in the proximal area. According to petrographic and SEM results, albite is present in all different rock types with different grades of mineralization. Albite alteration overprints the previous garnet alteration (Figure 9b, upper right corner), which suggests that albite alteration postdates garnet alteration. The relationships between mineralization and albite alteration in different rock types are currently uncertain due to the ubiquitous nature of albite alteration across all rock types.

Future Work

The other two major rock types at the Lorraine deposit are monzonite and monzodiorite; these should also be characterized using the same process as relied upon in this study. More detailed petrographic and geochemical analysis on alteration minerals should be completed to help define the origins of different generations of alteration minerals and their relationships to mineralization. Summarizing the characteristics of each alteration type in each of the different rock types will help to unravel the magmatic and hydrothermal processes that led to the formation of the Lorraine deposit.

Conclusions

Pyroxenite and syenite were classified in this study based on the proportion of K-feldspar, diopside and other mafic minerals. Pyroxenite is subdivided into biotite clinopyroxenite and feldspathic biotite clinopyroxenite. Syenite is subdivided into leucocratic, mesocratic and melanocratic syenite. Several possible alteration minerals are characterized and compared with previous studies:

- Biotite is subdivided into three texturally and geochemically different types; only the biotite present in leucocratic syenite is suggested to correlate with mineralization.
- Epidote-garnet alteration is more common than previously documented and, when compared with previous studies, shows strong correlations with mineralization. Characteristics of this alteration are most consistent with pre- or synmineralization timing and the epidote-garnet assemblage might prove to be a new vector for copper exploration at the Lorraine deposit.
- Albite alteration is ubiquitous in all rock types, with albite replacing garnet, but the timing relative to mineralization is uncertain.

Acknowledgments

The authors would like to thank Geoscience BC, Teck Resources Limited, NorthWest Copper Corp. and the Mineral Deposit Research Unit of the University of British Columbia for financially supporting this project. They would also

like to thank J. Lang, G. Titley and S. Peacock for reviewing the manuscript.

References

Bath, A.B. (2010): Geology, geochronology and alteration of the Lorraine alkalic porphyry Cu-Au deposit, British Columbia, Canada; Ph.D. thesis, University of Tasmania, 299 p., URL <https://doi.org/10.25959/23234834.v1>.

Bath, A.B., Cooke, D.R., Friedman, R.M., Faure, K., Kamenetsky, V.S., Tosdal, R.M. and Berry, R.F. (2014): Mineralization, U-Pb geochronology, and stable isotope geochemistry of the Lower Main zone of the Lorraine deposit, north-central British Columbia: a replacement-style alkalic Cu-Au porphyry; Economic Geology, v. 109, no. 4, p. 979–1004, URL <https://doi.org/10.2113/econgeo.109.4.979>.

Bissig, T. and Cooke, D.R. (2014): Introduction to the Special Issue devoted to alkalic porphyry Cu-Au and epithermal Au deposits; Economic Geology, v. 109, no. 4, p. 819–825, URL <https://doi.org/10.2113/econgeo.109.4.819>.

Bouzari, F., Hart, C.J.R., Bissig, T. and Barker, S. (2016): Hydrothermal alteration revealed by apatite luminescence and chemistry: a potential indicator mineral for exploring covered porphyry copper deposits; Economic Geology, v. 111, no. 6, p. 1397–1410, URL <https://doi.org/10.2113/econgeo.111.6.1397>.

Cooke, D.R., Wilson, A.J., House, MJ., Wolfe, R.C., Walshe, J.L., Lickfold, V. and Crawford, A.J. (2007): Alkalic porphyry Au–Cu and associated mineral deposits of the Ordovician to Early Silurian Macquarie Arc, New South Wales; Australian Journal of Earth Sciences, v. 54, no. 2–3, p. 445–463, URL <https://doi.org/10.1080/08120090601146771>.

Devine, F.A.M., Chamberlain, C.M., Davies, A.G.S., Friedman, R. and Baxter, P. (2014): Geology and district-scale setting of tilted alkalic porphyry Cu-Au mineralization at the Lorraine deposit, British Columbia; Economic Geology, v. 109, no. 4, p. 939–977, URL <https://doi.org/10.2113/econgeo.109.4.939>.

Kwan, K. and Müller, D. (2020): Mount Milligan alkalic porphyry Au-Cu deposit, British Columbia, Canada, and its AEM and AIP signatures: implications for mineral exploration in covered terrains; Journal of Applied Geophysics, v. 180, art. 104131, URL <https://doi.org/10.1016/j.jappgeo.2020.104131>.

Lang, J.R., Stanley, C.R., Thompson, J.F.H. and Dunne, K.P.E. (1995): Na-K-Ca magmatic-hydrothermal alteration in alkalic porphyry Au-Cu deposit, British Columbia; Mineralogical Association of Canada, Short Course Handbook, v. 23, p. 339–366.

Jamtveit, B. (1991): Oscillatory zonation patterns in hydrothermal grossular-andradite garnet: nonlinear dynamics in regions of immiscibility; American Mineralogist, v. 76, no. 7–8, p. 1319–1327.

Jamtveit, B., Agnarsdottir, K.V. and Wood, B.J. (1995): On the origin of zoned grossular-andradite garnets in hydrothermal systems; European Journal of Mineralogy, v. 7, no. 6, p. 1399–1410, URL <https://doi.org/10.1127/ejm/7/6/1399>.

Le Maitre, R.W. (2002): Igneous rocks: a classification and glossary of terms–recommendations of the International Union of Geological Sciences, Subcommission on the Systematics of Igneous Rocks (2nd edition); R.W. Le Maitre, A. Streckeisen, B. Zanettin, M.J. Le Bas, B. Bonin and P. Bateman (ed.), Cambridge University Press, p. 22–28, URL <https://doi.org/10.1017/CBO9780511535581>.

Mudd, G.M. and Jowitt, S.M. (2018): Growing global copper resources, reserves and production: discovery is not the only control on supply; Economic Geology, v. 113, no. 6, p. 1235–1267, URL <https://doi.org/10.5382/econgeo.2018.4590>.

Mudd, G.M., Weng, Z. and Jowitt, S.M. (2013): A detailed assessment of global Cu resource trends and endowments; Economic Geology, v. 108, no. 5, p. 1163–1183, URL <https://doi.org/10.2113/econgeo.108.5.1163>.

Müller, D. and Groves, D.I. (2019): Implications for mineral exploration in arc environments; *in* Potassic Igneous Rocks and Associated Gold-Copper Mineralization, D. Müller and D. I. Groves (ed.), Springer International Publishing, p. 337–354, URL <https://doi.org/10.1007/978-3-319-92979-8_10>.

Nixon, G.T. and Peatfield, G.R. (2003): Geological setting of the Lorraine Cu-Au porphyry deposit, Duckling Creek syenite complex, north-central British Columbia; BC Ministry of Energy, Mines and Low Carbon Innovation, BC Geological Survey, Open File 2003-4, 24 p.

Ootes, L., Bergen, A.L., Milidragovic, D., Jones, G.O., Camacho, A. and Friedman, R. (2020): An update on the geology of northern Hogem batholith and its surroundings, north-central British Columbia; *in* Geological Fieldwork 2019, BC Ministry of Energy, Mines and Low Carbon Innovation, BC Geological Survey, Paper 2020-01, p. 25–47.

Schlesinger, M.E., King, M.J., Sole, K.C. and Davenport, W.G. (2011): Production and use; Chapter 2 *in* Extractive Metallurgy of Copper (5th edition), M.E. Schlesinger, M.J. King, K.C. Sole and W.G. Davenport (ed.), Elsevier, p. 13–30, URL <https://doi.org/10.1016/B978-0-08-096789-9.10002-2>.

Schipper, B.W., Lin, H.-C., Meloni, M.A., Wansleeben, K., Heijungs, R. and van der Voet, E. (2018): Estimating global copper demand until 2100 with regression and stock dynamics; Resources, Conservation and Recycling, v. 132, p. 28–36, URL <https://doi.org/10.1016/j.resconrec.2018.01.004>.

Sillitoe, R.H. (2010): Porphyry copper systems; Economic Geology, v. 105, no. 1, p. 3–41, URL <https://doi.org/10.2113/gsecongeo.105.1.3>.